WCTE 2020
WORLD CONFERENCE ON TIMBER ENGINEERING
SANTIAGO, CHILE | 24 - 27 AUGUST

Equivalent Lateral Force Procedure for a Building with a Self-Centering Rocking Story of Cross-Laminated Timber (CLT) Walls

Marco Lo Ricco[1], Douglas R. Rammer[1], M. Omar Amini[1], Al Ghorbanpoor[2], Shiling Pei[3], and Reid B. Zimmerman[4]

ABSTRACT: The Equivalent Lateral Force (ELF) procedure is the most widely used seismic analysis approach, because of its simplicity and practicality in preliminary and final design phases. This paper applies the ELF procedure to a hypothetical building that stands 5 stories tall, with a 4-story superstructure supported on a rocking story of elliptically profiled cross-laminated timber (CLT) walls. First-generation prototypes made from six CLT panels of 5-ply, 175 mm, thickness—each measuring 2.44 m by 3.66 m in respective width and height—demonstrated that elliptical geometry controls lateral stiffness, inherent damping, and self-centering of the walls. Full-scale, cyclic, quasi-static, lateral-load-displacement tests—under simulated gravity loads ranging from 133 to 400 kN—established effective stiffness and damping inputs for the ELF procedure. The prototypes produced two modes of elliptical pendulum response by changing steel connections to the floor and ceiling beams. The first connection guides panels through rolling, and the second connection forces panels into slip-friction for enhanced damping but reduced durability of CLT. Because the base rocking story of elliptically profiled CLT walls behaves like an inverted pendulum system, the ELF procedure references existing design provisions for seismically isolated structures.

KEYWORDS: Equivalent Lateral Force (ELF) procedure, seismic isolation, rocking story, pendulum, cross-laminated timber (CLT)

1 INTRODUCTION

Over a decade ago, mass timber construction rose to international prominence with superstructures primarily made of cross-laminated timber (CLT) panels. Crews of few on-site workers rapidly erected structures up to 9 stories tall, facilitated by prefabricated CLT panels of robust sizes that functioned versatilely as loadbearing walls or slabs. 3D seismic shake-table testing of 3- and 7-story CLT structures built to full-scale, Ceccotti et al. [1, 2] showed that such fully panelized archetypes can withstand simulated earthquakes. Horizontal accelerations, however, exceeded 3g at a top floor and revealed a need to alleviate rigidity of this efficient assembly type. Since pioneering these CLT forms, the producers and archetypes of mass timber buildings have expanded globally. Because many sizable timber construction hubs coincide with seismicity, around the world, continued development of seismic mitigation strategies for mass timber remains a priority for growth.

1.1 SEISMIC DEVELOPMENT STRATEGY

For broad applicability in North America, Pei et al. [3, 4] mapped a comprehensive strategy to develop CLT structures for an array of performance objectives. By outlining multiple tiers of seismic performance, the Pei et al. (2014, 2016) roadmap for structural research opened several pathways to building code conformance in the United States. Amini et al. [5] developed a multistory CLT construction system of platform-framed shearwalls and determined the seismic performance factors via the rigorous and recently implemented FEMA P695 [6] methodology—which involves prototype testing, archetype development, dynamic nonlinear analysis, and peer review to quantify the seismic performance factors most widely referenced by structural building code provisions.

Pei et al. [7] led similar efforts to develop prototypes and archetypes of mass timber structures, laterally supported by vertically post-tensioned CLT rocking walls, for next-generation Performance-Based Seismic Design (PBSD) procedures that aim for earthquake resiliency. Pei et al.

[1] Marco Lo Ricco, USDA, Forest Service, Forest Products Laboratory, Madison, WI, United States, marco.loricco@usda.gov

Douglas R. Rammer, USDA, Forest Service, Forest Products Laboratory, Madison, WI, United States, douglas.r.rammer@usda.gov

M. Omar Amini, USDA, Forest Service, Forest Products Laboratory, Madison, WI, United States, mohammad.amini@usda.gov

[2] Al Ghorbanpoor, Department of Civil & Environmental Engineering, University of Wisconsin—Milwaukee, United States, algh@uwm.edu

[3] Shiling Pei, Department of Civil & Environmental Engineering, Colorado School of Mines, Golden, CO, United States, spei@mines.edu

[4] Reid B. Zimmerman, KPFF Consulting Engineers, Portland, OR, United States, reid.zimmerman@kpff.com

[8] tested a full-scale 2-story mass timber structure laterally supported by vertically post-tensioned walls of CLT to demonstrate resiliency of such a rocking system. 3D shake-table tests of a 10-story version are planned for 2021 [9].

1.2 CONTROLLED ROCKING

Whether striving for enhanced ductility or resiliency in earthquake mitigation, controlled rocking has proven effective for inherently rigid panels. To explain how rigid structures of seemingly unstable proportions had survived devastating earthquakes, Housner mathematically demonstrated that dynamic pulses could excite tall and slender rigid blocks into inverted pendulum motion [10]. Despite this breakthrough in mechanics, ways to control rocking in the design of earthquake-resistant buildings developed decades later. Eventually, the precast concrete industry made use of rocking mechanisms with restraints, like vertical and unbonded post-tensioning, and a variety of energy-dissipating connections that engaged when gaps opened at panel joints [11]. Based on historical development and recently proven performance, rocking wall adaptations to mass timber prevail in current research [12-14]. Unlike ductile yielding, which produces permanent inelastic deformation by design, pendulum oscillations settle to an original equilibrium position that produces negligible residual displacement. Rocking thus offers intrinsic seismic resiliency not found in other lateral force-resisting systems.

1.3 SEISMIC ISOLATION AND SOFT-STORY OBJECTIVES

This project uses ASCE 7-16 [15] Chapter 17 provisions of seismic isolation to develop controlled rocking of elliptically profiled CLT wall panels, because the prototyping and analysis requirements of the isolation standard provide a framework that achieves resiliency. Table 1, adapted from Chapter C17 of ASCE 7-16, compares the performance expectations of fixed-base and isolated buildings underlying the code provisions and shows that isolated buildings aspire to preserve structural and non-structural components, in addition to life safety.

This CLT system enlarges and elaborates the concept of *elliptical rolling rod isolation* [16] to create a rocking soft story as Figure 1 illustrates, for example.

***Table 1:** Comparison of Earthquake Performance Expectations*

	Earthquake Intensity [a]		
Performance	Minor	Moderate	Major
Life safety	F, I	F, I	F, I
Structural damage insignificant	F, I	F, I	I
Nonstructural damage insignificant	F, I	I	I

[a] F = fixed base; I = isolated.

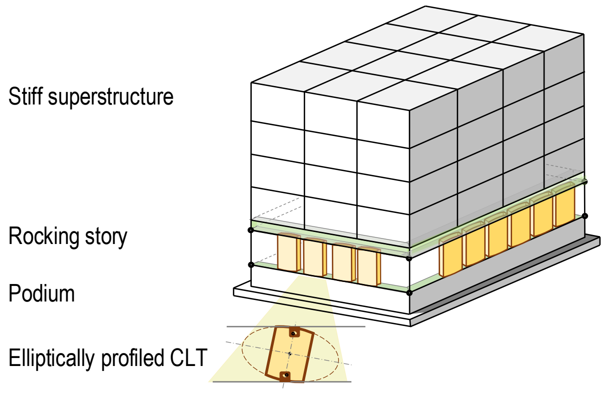

***Figure 1:** Diagram of stiff superstructure over rocking CLT story*

McVitty and Taylor [17] generally likened the concept of an engineered soft-story to seismic isolation, because both systems concentrate large displacements at a single horizontal plane to buffer the superstructure from seismically induced forces. Whether establishing the isolation plane with compact bearings or story-tall components, the engineered system must (a) maintain stability when subject to design displacements in various directions, (b) inherently develop a restoring force that increases resistance with increasing lateral displacement, (c) sustain cyclic lateral loading without significant degradation, and (d) exhibit predictable lateral force-deflection characteristics and damping [15]. This paper first addresses the theory and prototype testing used to determine engineering properties of the elliptically profiled CLT rocking wall system and then presents an example of the Equivalent Lateral Force (ELF) analysis procedure, to highlight isolation requirements specific to elliptical rocking wall panels. The results show the implications of two different mechanisms of story shear transfer and geometric proportioning on the isolation, damping, and lateral displacements of the elliptically profiled systems. Finally, this paper addresses wind restraints and other resolvable dilemmas that seismic isolation systems commonly encounter.

2 ANALYSIS MODELS

Jangid and Londhe [16] proposed *elliptical rolling rod isolation* decades ago, as a compact bearing system placed beneath a multistory superstructure. Their model numerically demonstrated the effectiveness of various ellipse eccentricities as inverted pendulum isolators. Londhe and Jangid [18] later developed expressions to distinguish non-rolling, rolling, and sliding conditions between the elliptical rolling rods and bounding horizontal planes of the foundation and superstructure. Practical application, however, requires more details of story shear transfer.

This newly developed CLT version of the elliptical pendulum concept addresses several practical matters. First, realizing only a middle portion of an ellipse provides an adequate range of displacement capacity. (i.e. ellipse ends may be truncated as shown by the dashed lines of Figures 1 and 2.) Second, the project team identified two primary mechanisms of shear transfer that lead to either *No-Slip Traction Rolling* (NSTR) or *Slip-Friction Rocking* (SFR) modes of pendulum behavior, diagrammed in Figure 2.

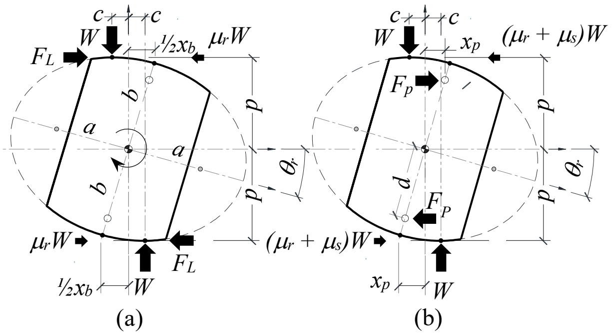

Note: *Minor forces, such as panel weight, not shown*

Figure 2: *Free-Body Diagrams of (a) NSTR and (b) SFR*

Subtle differences between the free-body diagrams of Figure 2 significantly vary the stiffness, damping, and connection details of NSTR and SFR.

2.1 NO-SLIP TRACTION ROLLING (NSTR)

The free-body diagram (FBD) of Figure 2a most closely resembles the conditions of rolling that Jangid and Londhe [16] had assumed. It shows lateral force transfer, F_L, applied at the edges of the panel. A counteracting frictional force—the product of rolling friction coefficient, μ_r, and superstructure weight, W—adds damping. Rotation, θ_r, governs the rolling system as the independent degree of freedom. Panel rotation laterally displaces the superstructure a total distance, x_b, and raises or lowers the superstructure strictly vertically (a condition met with proper layout of walls to prevent superstructure rotation). In the plumb panel position, the distance between floor and ceiling beams measures the height of the ellipse, $2b$, and increases to $2p$, as the panel rotates. For rigid-body motion (neglecting small displacements in the panel and bounding beams), the total vertical displacement of the superstructure, therefore, may be computed as $2p$ minus $2b$. The moment arm distance, $2c$, between panel contact points, increases with rotation, so restoring moment acts proportionally with lateral displacement.

Major axis width, $2a$, and minor axis height, $2b$, of the profiling ellipse factor into the geometric relationships, based on an assumption fundamental to rolling; the horizontal length of rolling equates to distance traveled along the elliptical arc (i.e., no slip occurs). Jangid and Londhe [16] provide details of the geometric derivations, which involve an elliptic integral to determine arc length. Resolving the geometric relationships and forces acting on the panel in Figure 2a, yields the lateral force estimate of Equation 1:

$$F_L = W\left(\mu_r sgn(\dot{x}_b) + \frac{c}{p}\right)x_b \tag{1}$$

where F_L = lateral force; W = gravity load of effective seismic weight; μ_r = rolling friction coefficient; sgn = signum function; x_b= lateral displacement and $\dot{x}_b$ = the derivative of the rocking story velocity; c = half the moment arm distance between contact points at load-bearing panel edges, and p = half the height between floor and ceiling.

Figure 3 plots the lateral force-displacement hysteresis of the panel diagrammed in Figure 2a, and idealized by Equation 1, with 3 cycles of measured test data. The prototype test apparatus applied lateral displacement cycles and 400 kN (90 kips) of vertical load that represented W to a CLT panel profiled with an ellipse of semi-major axis width, a, of 2350 mm (92.5 in.) and semi-minor axis width, b, of 1829 mm (72 in.), with simulated boundary conditions of Figure 2a. Looking at the figure, the idealized NSTR model matched data reasonably well, with a rolling friction coefficient, μ_r, assumed as 1 percent.

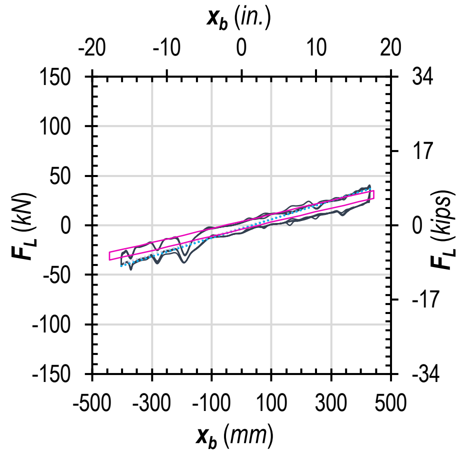

Figure 3: *Lateral Force-Displacement Hysteresis of NSTR*

Slip of the wall at the floor or ceiling contact surfaces would compromise self-centering of the rolling pendulum with residual displacements. NSTR therefore requires adequate traction for rolling and a way to preclude slip. The exploded diagram of Figure 4 illustrates the prototype assembly designed to serve as a dual-purpose *displacement restraint* that limits slip and the extents of lateral displacements, using slotted pin connections.

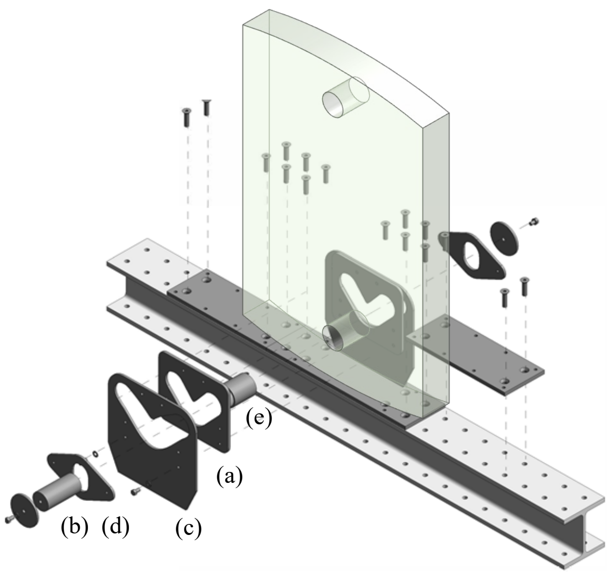

Figure 4: *Exploded assembly of steel beam and CLT for NSTR*

In Figure 4, plates (a) confined pin (b) within V-shaped slots. The V-shape traces a path of pin travel that is specific to a rolling ellipse profile, so plates (a) were made for interchangeability of CLT panels during prototype testing. The cutout of plates (c) enveloped the V-shaped slots of 6 elliptical panel profiles illustrated in Table 3, so that plates (c) could be fixed via welds to track plates that bolted to a steel beam. Plates (d) initially locked the pins in place with sacrificial notched bolts. Steel pin (b) slid through all plates and pipe bushing (e) embedded in the CLT panel. Because the slots were shaped to engage only if the panel slipped or rotated too far, NSTR connections transferred only incidental forces during prototype tests.

2.2 SLIP-FRICTION ROCKING (SFR)

Figure 2b modified the rolling system to actively transfer lateral forces, F_P, through horizontally constrained pins. Active force transfer through the pins shortens the moment arm between F_P forces of FBD (b), relative to the moment arm between F_L forces of FBD (a). Horizontal constraint of the pins adds sliding, denoted by coefficient μ_s, to the frictional damping forces acting on the edges of the panel. In *SFR,* CLT panels roll and slide simultaneously, because the vertically slotted connection plates of Figure 5 constrain horizontal movement of the pins.

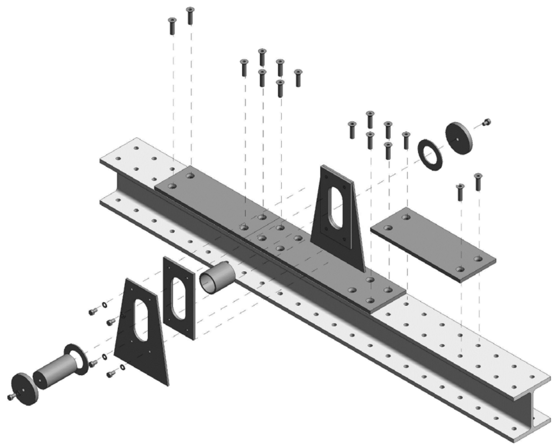

Figure 5: *Exploded assembly of steel connection for SFR*

Vertical slots forced shear transfer to occur primarily through bearing among the pin and plates and CLT bushing pipe. Though SFR and NSTR exhibit the same rotational capacity, θ_r, the total lateral translation, $2x_p$, of SFR must always be less than the total lateral translation, x_b, of NSTR, because of connection constraint. Lo Ricco et al. [19] derived Equation 2 to quantify effects of a shorter moment arm between story shears through the pins and frictional sliding resistance, in addition to rolling.

$$F_p = W\left((\mu_r + \mu_s) sgn(\dot{x}_p)\frac{c}{d\cos\theta_r}\left(\frac{2p}{d\cos\theta_r} - 1\right)\right)x_p \qquad (2)$$

where F_p = lateral force traveling through pins; μ_s = sliding friction coefficient; x_p = lateral displacement and $\dot{x}_p$ = the derivative of the rocking story velocity with added horizontal pin constraint; d = distance between wall panel centroid to pin center, and θ_r = rotation of the elliptical panel.

Figure 6 plots the lateral force-displacement hysteresis of the panel diagrammed in Figure 2b and idealized by Equation 2, with 3 cycles of measured test data.

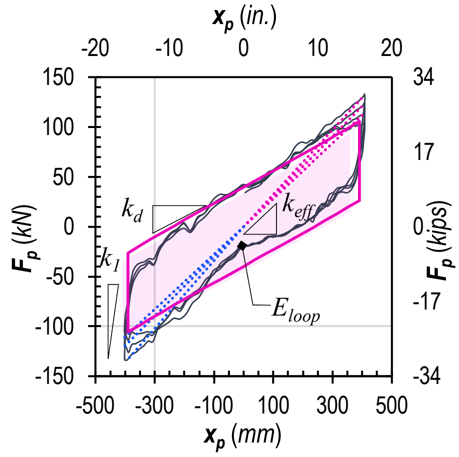

Figure 6: *Lateral Force-Displacement Hysteresis of SFR*

All aspects of the panel corresponding to the hysteresis of Figure 6 match the panel corresponding to Figure 3. In fact, prototype testing of both NSTR and SFR configurations used the same CLT panel and swapped the vertically slotted SFR connection plates of Figure 5 for the V-slotted NSTR restraints of Figure 4 in respective tests. Like Figure 3, Figure 6 presents lateral load-displacement under an applied vertical load, *W*, of 400 kN (90 kips). Both figures, furthermore, use the same scale to facilitate visual contrast. SFR clearly generates more area within the hysteresis loops, labeled E_{loop} in Figure 6 for energy dissipated per cycle. Equation 2 accounts for this energy increase by estimating a sliding friction coefficient, μ_s, equal to 9 percent, so that sliding and rolling coefficients sum to 10 percent.

For practical engineering analysis, Figures 3 and 6 are used to calculate effective stiffness and damping respective to NSTR and SFR. Though based on nonlinear equations, both lateral force-displacement plots show that the idealized hysteresis resembles the bilinear force-deflection model referenced in ASCE 7-16 [15] Chapter 17 provisions for determining isolator characteristics. The three slopes in Figure 6 illustrate various stiffness computations derived from test data. Linear fitting along the loading and unloading branches of the hysteresis data determines slope k_d, which corresponds with the stiffness that Equation 2 predicted using mechanics. A linear slope fitting the nearly vertical legs of the hysteresis loop determines k_1, stiffness in the reversal from loading to unloading at extreme displacements of the hysteresis cycle. Slope k_{eff} determines effective stiffness, for practical assessment of system performance. Changes to k_{eff}, as seen over the 3 cycles plotted in Figure 6, warrants review of the system for damage, like Figure 9 shows.

Effective stiffness, k_{eff}, depends on the magnitude of displacements and corresponding forces at the maximum positive and negative excursions of the hysteresis cycle, as computed by Equation 3:

$$k_{eff} = \frac{|F^+| + |F^-|}{|\Delta^+| + |\Delta^-|} \qquad (3)$$

where lateral forces F+ and F- correspond with the positive Δ^{+} and negative Δ^{-} maximum-magnitude displacements of the hysteresis cycle [15].

Determining effective stiffness, in turn, enables computation of effective damping, B_{eff}, according to Equation 4:

$$B_{eff} = \frac{2}{\pi} \frac{E_{loop}}{k_{eff}(|\Delta^{+}| + |\Delta^{-}|)^2} \tag{4}$$

where E_{loop}, sums the area enclosed by each lateral force-deflection hysteresis cycle to determine the amount of energy dissipation [15].

2.3 EQUIVALENT LATERAL FORCE (ELF) ANALYSIS

ELF is the most practical analysis approach, because the procedure simplifies the dynamic effects of earthquakes into statically applied forces. ELF analysis has long served the design of fixed-base buildings, and ASCE 7-16 [15] Chapter 17 provisions for isolated buildings include considerations specific to isolated buildings. McVitty and Taylor [17] summarize a design procedure for isolated structures that references ELF in 5 of the 7 steps. The following example carries out the first few steps of the procedure to compare NSTR and SFR performance based on preliminary layouts and estimates.

2.3.1 Objectives

The Pacific Northwest region of the United States is home to a timber construction industry that has erected several notable mass timber buildings in a region of significant seismicity. Through ELF analysis, this example of a Risk Category II building compares NSTR and SFR rocking wall configurations for a Site Class C location in Portland, Oregon. Table 2 summarizes the seismic hazard values [20]. Building code requirements for isolated structures focus on the Risk-targeted Maximum Considered Earthquake, MCE_R, event. This example will demonstrate a range of workable rocking wall options, for comparison with a fixed-base building.

Table 2: *Spectral response acceleration parameters (SRAPs)*

Parameter	Value	Description
S_s	0.884	mapped MCE_R, 5% damped, SRAP at short periods (0.2 s)
S_1	0.396	mapped MCE_R, 5% damped, SRAP at a period of 1.0 s
S_{MS}	1.061	the MCE_R, 5% damped, SRAP at short periods (0.2 s) adjusted for site class effects
S_{M1}	0.594	the MCE_R, 5% damped, SRAP at a period of 1.0 s adjusted for site class effects
S_{DS}	0.707	design, 5% damped, SRAP at short periods (0.2 s)
S_{D1}	0.396	design, 5% damped, SRAP at a period of 1.0 s

2.3.2 Scope and Limitations of Prototypes

Jangid and Londhe [16, 18] numerically analyzed dynamic responses of a moment-frame structure with rigid floor masses atop elliptical rolling rods, excited with historical records of earthquakes. They showed that ellipse eccentricity, e, expressed by Equation 5 in terms of semi-major and -minor axis lengths a and b, respectively, controlled stiffness of the system.

$$e = \sqrt{\frac{a^2 - b^2}{a^2}} \tag{5}$$

Ellipses with low eccentricity reduced base shear of the superstructure, V_b, but with greater peak lateral displacements in the rocking story. More oblate ellipses produced lesser peak lateral displacements but increased base shear, V_b. When e = 0, the ellipse is a circle with no resistance to lateral load. When e = 1, the wall panel essentially becomes rectangular. To test effects of geometric proportioning at the scale of a one-story-tall wall, this study prototyped the panels and connections of Table 3, for cyclic lateral displacement-controlled testing.

Table 3: *Prototype test matrix*

1 constant rectangular CLT 5-ply [a] panel size

2.44 m × 3.66 m (8 ft × 12 ft)

× 6 ellipse profiles of varying eccentricity, e

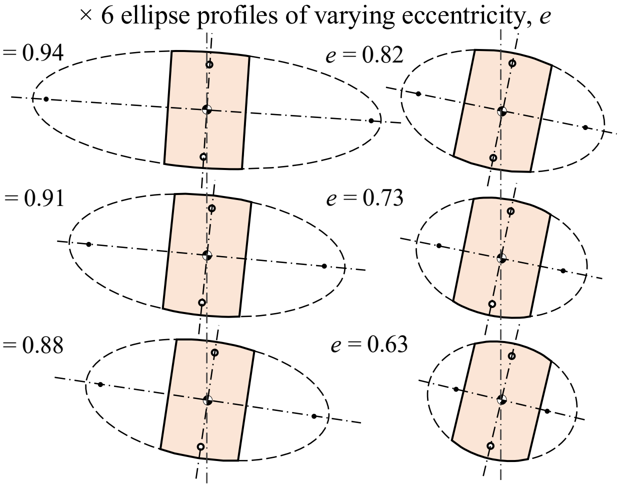

Illustrated at maximum rotations

× 2 connection configurations

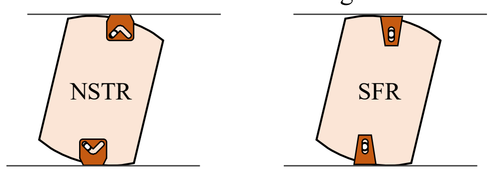

Figures 2a & 4 | Figures 2b & 5

× 3 weights, W [c]

133 kN | 267 kN | 400 kN

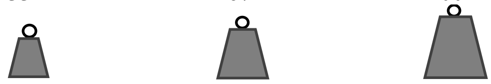

= 36 cyclic displacement protocols planned [b]

[a] Total panel thickness = 170 or 175 mm due to change in planing face laminations between CLT production runs

[b] SFR could not complete extreme cycles under medium and high W, because of CLT damage near pins

[c] Gravity simulated by synchronized vertical actuators

ASCE 7-16 [15] Chapter 17 requirements for prototype testing are written for direct application to building projects. The standard protocols express seismic displacement steps for each test cycle as fractions of the maximum lateral translational displacement, D_M, of the center of rigidity for an isolator layout. At $0.75D_M$ the standard requires site-specific parameters S_{M1} and S_{MS} to determine if more than 10 cycles are required to demonstrate durability. The site parameters listed in Table 2, for example, prescribe 17 cycles at the $0.75D_M$ load step. The standard, furthermore, requires tests under 3 load combinations to determine whether uplift or additional weight on isolators has an appreciable effect on stiffness, damping, or stability. Therefore, each of these displacement, durability, and stability requirements needs a known building design and site location.

For a generalized approach, we substituted the weights of Table 3 for design load combinations and maximum lateral displacement capacity of an individual wall component, δ_M, for D_M. Figure 7 shows the cyclic protocol in terms of δ_M, which varies for each of the 6 elliptical profiles of Table 3 with the safe rotational capacity (determined by contact of the corners) illustrated by the test matrix. For a given ellipse eccentricity, NSTR and SFR panels have the same rotational capacity, but the vertically slotted connections of SFR imposed a horizontal pin constraint that reduces δ_M by the magnitudes plotted in Figure 7.

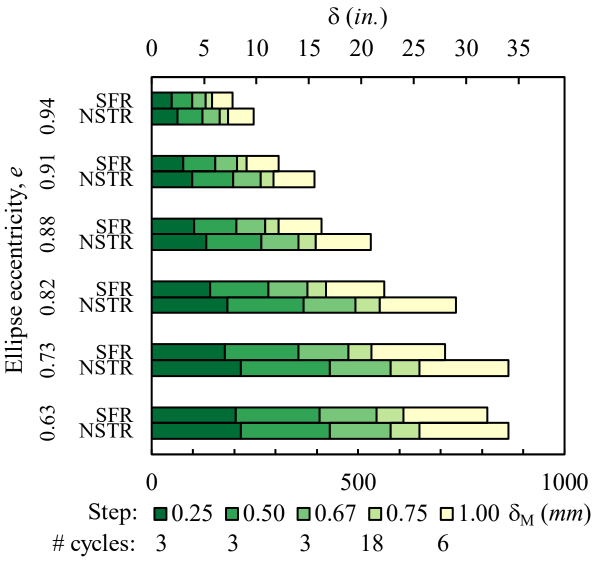

Figure 7: *Cyclic lateral displacement of quasi-static protocols*

Figure 8 pictures the test setup. Horizontally oriented actuators (a), stacked in series for cyclic displacements up to ±432 mm (17 in.), pushed or pulled to roll bottom beam (b) along a linear track mounted to the floor. Vertically oriented actuators (c) stroked synchronously to level and roll the top beam (d) along columns, while the actuators maintained a constant sum of load as the contact point traveled along the top beam span. For lateral displacement steps up to 432 mm (17.0 in.), the apparatus could apply fully reversed cycles, displacing the panel nearly equally left and right of the plumb position. For greater lateral displacements, the apparatus was reconfigured to displace from the plumb position only in one direction.

Figure 8: Prototype test setup

Throughout tests, NSTR protected panels from significant damage. In contrast, SFR damaged CLT around the pin bushings and wore out the loadbearing edges, as shown in Figure 9. Therefore, many SFR protocols under medium and high weight could not be completed [19, 21]. Nonetheless, this example assumes that SFR behaves as idealized in Figure 6, with broader distribution of forces at pins and edges. The first-generation prototypes reserved many practical details, like wind restraints, to focus on seismic behaviors of the rolling wall pendulum. The prototypes, moreover, only tested bearing contact surfaces of softwood CLT and unpainted hot-rolled steel plates in a conditioned lab environment. The ASCE 7-16 [15] Chapter 17 isolation standard requires dynamic testing of such practical details to envelope displacements and forces transferred by the system in analysis. Therefore, first-generation prototypes provide a substantial but limited basis for the following ELF analysis example. Particularly for SFR, more practical development is required prior to construction of elliptically rocking soft stories in actual buildings.

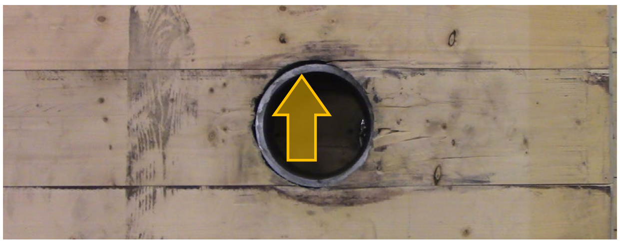

(a) Hole elongation around steel bushing

(b) Edge wear of 3 panels

Figure 9: *Damage observed after SFR tests*

2.3.3 Conditions of ELF Applicability

ASCE 7-16 [15] Chapter 17 places seven main conditions on ELF for use as a final analysis procedure in the design of isolated structures. This example complies with the following limitations.

1. Site Class must fall within the range of A to D.
2. The effective period of the of the isolated structure, T_M, must fall below 5.0 seconds.
3. The supported structure must be limited to 19.81 m (65 ft) in height, or 4 stories, though the code permits exceptions if overturning effects on the superstructure avoid placing any of the isolators into net tension. Figure 1, therefore, presents a 4-story superstructure over a rocking story, for a building that rises a total of 5 stories.
4. Effective damping of the isolation system must not exceed 30 percent.
5. The effective period at maximum displacement, T_M calculated by Equation 6, must exceed the elastic fixed-base period of the structure by at least 3 times.

$$T_M = 2\pi \sqrt{\frac{W}{k_M g}} \tag{6}$$

where k_M = effective stiffness at maximum lateral displacement and g = gravitational acceleration. In other words, the rocking story must support a relatively rigid superstructure. In the absence of data specific to a CLT buildings, Equation 7, from ASCE 7-16 [15] Chapter 12, approximates the fundamental period.

$$T_a = C_t h_n^x \tag{7}$$

where C_t = 0.0488 (metric), 0.02 (U.S. units) and x = 0.75 for all structural systems, other than the steel and concrete systems specified in ASCE 7-16 [15] Table 12.8-2, and h_n = structure height. Providing a relatively rigid superstructure to meet this relative period requirement enhances effectiveness of the isolation.

6. The superstructure must be regular.
7. The isolation system has:
   a. Effective stiffness, k_M, at maximum displacement, D_M, greater than one-third the effective stiffness at $0.20D_M$, to prevent excessive softening.
   b. Lateral restoring force at D_M that exceeds the lateral force at $0.5D_M$ by at least $0.025W$, for reliable self-centering. Ellipse eccentricity, as discussed previously, must be great enough to act as a pendulum, rather than a circular roller.
   c. Freedom to displace through the total maximum displacement, D_{TM} equal to the sum of translational and torsional displacements, before engaging restraints.

Figure 10 shows a regular scheme of rolling pendulum walls, with panels forming a core and perimeter. The diagram superposes translational D_M and total D_{TM} effects that story shear, V_b, and eccentricity, e_r, generate. Equations 8, 9 and 10 respectively calculate D_M, D_{TM}, and k_M of the rocking story.

$$D_M = \frac{g S_{M1} T_M}{4\pi^2 B_M} \tag{8}$$

where B_M = numerical coefficient for the effective damping of the isolation system β_M at the displacement D_M, as provided in ASCE 7-16 [15] Table 17.5-1.

$$D_{TM} = D_M \left[1 + \left(\frac{y}{P_T^2}\right) \frac{12 e_r}{b^2 + d^2}\right] \tag{9}$$

where y = the distance between centers of rigidity of the isolation system and the element of interest measured perpendicular to the direction of seismic loading;

e_r = the actual eccentricity measured in plan between the center of mass of the superstructure and center of rigidity of the soft-story, plus accidental eccentricity taken as 5% of the longest plan dimension of the structure perpendicular to the direction of force under consideration;

b = the shortest plan dimension of the structure measured perpendicular to d;

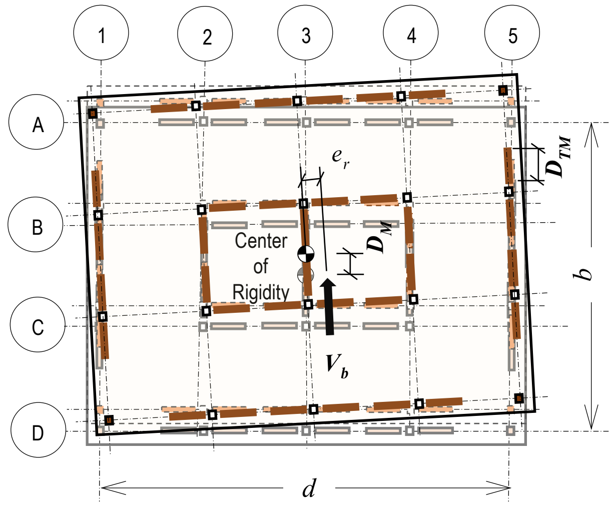

d = 4 Equal spaces @ 7.315 m (24 ft) = 29.261 m (96 ft)
b = 3 Equal spaces @ 7.315 m (24 ft) = 25.946 m (72 ft)
$e_r = 0.05d$ + distance between centers of rigidity and mass

Figure 10: Plan view of laterally displaced rocking story

P_T = ratio of effective translational period of the isolation system to effective torsional period of the isolation system, which need not be less than 1.0. ASCE 7-16 [15] Chapter 17 provides an approximate method of determining this period ratio, for use prior to dynamic analysis.

$$k_M = \frac{\sum|F_M^+| + \sum|F_M^-|}{2D_M} \tag{10}$$

where

$\sum F_M^+$ = sum for all isolator units of the absolute value of force at a positive displacement equal to D_M.

$\sum F_M^-$ = sum for all isolator units of the absolute value of force at a negative displacement equal to D_M.

In the building layout of Figure 1, the 4-story superstructure height, h_n from Level 2 through roof, measures 15.85 m (52 ft) tall, and the overall 5-story building rises to (65 ft) with 3.96 m (13 ft) of height allotted equally to each story. Table 3 provides an estimate of building weights at each level and the summation. ASCE 7-16 [15] Chapter 4 specifies live load intensities and reduction factors, R_1, for various occupancies and structural components.

The effective seismic weight of the superstructure structure includes the entire dead load and half of the reduced live load to yield *W* equal to 12,113 kN (2723 kips). Sizing thickness of individual CLT wall panels and other detailed design checks must include the load combinations specified in ASCE 7-16 [15], Chapter 17. Effective seismic weight *W* factors into the Equation 6 effective period calculation, T_M, which in turn influences maximum displacement, D_M, and effective stiffness, k_M, of the system.

Table 4: *Building weights*

Level	D (kN)	D (kips)	*L* (kN)	*L* (kips)	R_1
Roof	1117	251	646	145	0.611
5	1911	430	2541	571	0.562
4	1911	430	2541	571	0.562
3	1911	430	2541	571	0.562
2	2210	497	2541	571	0.562
∑	9060	2037	10,810	2429	

3 RESULTS

Figures 11 and 12 summarize the effective engineering properties, at the $0.50\delta_M$ step plotted in Figure 7, of 6 CLT panels prototyped in the Table 3 test matrix. Figure 11 plots the mean effective stiffness, with each k_{eff} data point representing 3 load trials of the Table 3 test matrix, by normalizing results to a unit of vertical load *W*. This normalization typically produced the same lateral stiffness values within a few percent error. Generally, lateral stiffness increased nonlinearly with ellipse eccentricity, with SFR further increasing stiffness relative to NSTR.

Figure 12 plots the effective damping results. Except for one outlier, the panel with least elliptical eccentricity, effective damping essentially equated to 5 percent for the NSTR configuration. As expected, SFR produced considerably more damping. In contrast to the relatively constant damping of NSTR, the damping of SFR varies nonlinearly and diminishes with increasing ellipse eccentricity. The sliding distance that panels must travel to rotate in SFR offers a plausible explanation. The vertically slotted plates of Figure 5, force panels of lesser eccentricity to slide greater distances through the rolling motion. Because frictional sliding was the predominant damping mechanism, less sliding produced less damping. The V-shaped slots of NSTR connections grew less pronounced as ellipse eccentricity increased, so more oblate profiles generally survived SFR longest in prototype tests, before succumbing to the damage photographed in Figure 9.

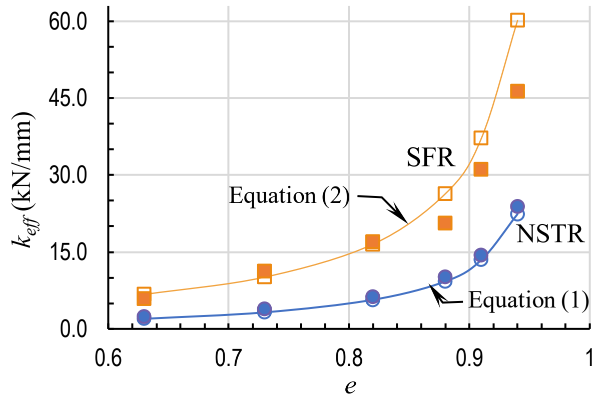

Figure 11: *Effective stiffness (W = 1.0 kN) at $0.5\delta_M$ of panels profiled to various ellipse eccentricities*

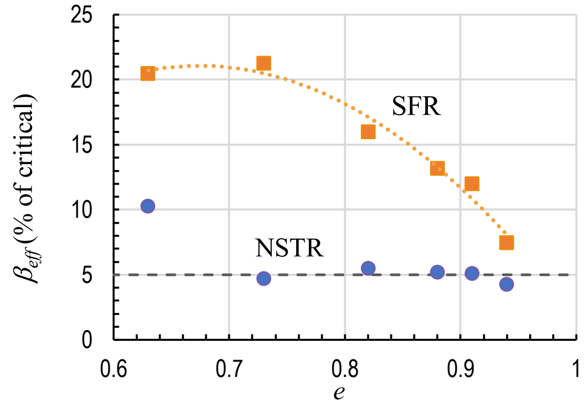

Figure 12: *Effective damping at $0.5\delta_M$ of panels profiled to various ellipse eccentricities*

Table 5 summarizes the results of one iteration of analysis, using the effective properties of Figures 11 and 12 to determine effective stiffness, k_M, and period, T_M, at maximum displacement, D_M. Among 12 computations, only the panel profiled to 0.82 ellipse eccentricity matched D_M and $0.5\delta_M$ on the first iteration. For the other 11 options, k_M must be recomputed using effective properties near the D_M tabulated here, until iterations converge. Prototype data at $0.25\delta_M$, for example, may lead to rapid convergence of the 0.73*e* SFR wall, because the first iteration of D_M equates to approximately $0.25\delta_M$. For displacements that fall between displacement steps of the testing protocols, idealized bilinear hysteresis models, like the generic fit or mechanical models of Equations 1 and 2, may estimate engineering properties.

Because approximate period, T_a, of the superstructure equals 0.4 seconds, the rocking system should aim for a period at least 1.2 seconds long. The 0.82*e* walls lengthened the period to 2.5 seconds with a lateral maximum displacement of 376 mm (14.8 in.). In configurations like Figure 10, torsional effects typically amplify displacement demands up to 15 percent [15]. This places D_{TM} within ample lateral displacement reach, δ_M, of the wall components. In addition to in-plane wall movement, walls of the rocking story must undergo out-of-plane displacements compatible with the magnitudes of D_M and D_{TM}. Flexible steel connections and profiling load bearing surfaces of CLT panels to eliminate abrupt corners are critical to stability during these large displacement excursions in both lateral directions. Biaxial testing is therefore needed to further validate this rocking story system of elliptically profiled walls.

Table 5: *Effective engineering properties at D_M*

	e	B_M [a]	k_M (kN/mm)	T_M (s)	D_M (mm)	$0.5\delta_M$ (mm)
NSTR	0.63	1.0	2.91	4.1	604	430
	0.73	1.0	4.72	3.2	474	434
	0.82	1.0	7.51	2.5	376	370
	0.88	1.0	12.23	2.0	295	267
	0.91	1.0	17.44	1.7	247	198
	0.94	1.0	28.95	1.3	192	124
SFR	0.63	1.5	7.15	2.6	257	408
	0.73	1.5	13.69	1.9	186	358
	0.82	1.4	20.59	1.5	165	283
	0.88	1.3	24.95	1.4	159	207
	0.91	1.3	37.67	1.1	133	154
	0.94	1.1	56.20	0.9	125	99
	See Equations		(10)	(6)	(8)	

[a] Linearly interpolated from ASCE 7-16 [15] Table 17.5-1

4 CONCLUSIONS

Figure 13 plots the MCE$_R$ response spectrum of Table 2 parameters and superposes the solution highlighted in Table 5 and approximate period of a fixed-base, 5-story building. The rocking story reduced spectral acceleration nearly 80% according to the ELF analysis. Though rolling isolation can achieve effective periods of 3 or 4 seconds, according to Table 5, the response spectrum shows less dramatic S_a reductions for longer periods beyond 2.5 seconds.

The ELF procedure readily determines the base shears of Table 6 for comparison of fixed-based and isolated schemes. For the isolated building, V_b acts at floor and ceiling levels of the rocking story, and V_{st} accumulates shear from the remaining upper floors and roof. Relative to the fixed-base building, the rocking story provides a 35% reduction in base shear. Table 1, however, reveals a major mismatch in this base shear comparison. For the fixed-base building to remain elastic at the *MCE$_R$* event, design must target roughly 3 times the tabulated base shear, V, to eliminate ductility. In other words, the reduction in base shear grows to approximately 75% for the rocking story building if the fixed-base structure targets a similar level of insignificant damage during the MCE$_R$ event.

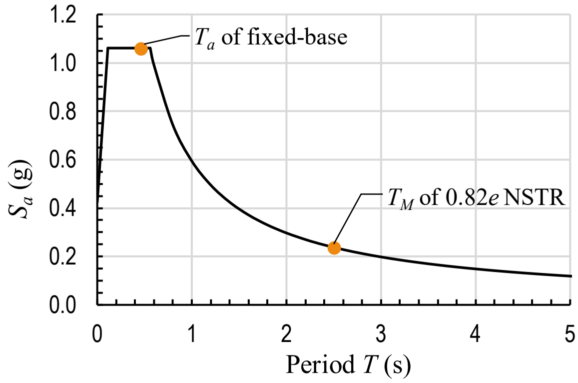

Figure 13: MCE$_R$ response spectrum

Table 6: Base shears determined by ELF for MCE$_R$

Fixed-Based (R = 3) V [a]		Rocking Story V_b		Superstructure V_{st}	
(kN)	(kips)	(kN)	(kips)	(kN)	(kips)
4285	963	2824	635	2218	499
(12.8-1)		(17.5-5)		(17.5-7)	

Bottom row references ASCE 7-16 [15] equation numbers.

[a] To calculate *V for MCE$_R$*, S_{MS} and S_{M1} substitute S_{DS} and S_{D1} in standard design earthquake equations.

R = Response Modification Coefficient

Equation 11 for shear applied to the rocking story captures the essence of isolation systems with a classic model of a spring. Therein lies the resiliency of the rolling elliptical system and power of simplicity in the ELF method of analysis.

$$V_b = k_M D_M \tag{11}$$

The rocking story apportions V_b to walls in the form of F_L or F_P respective to NSTR and SFR systems diagrammed in Figure 2. One connection constraint changed the role of friction, from the primary mechanism of shear transfer to a counteracting force that added damping. Because the magnitude of friction between the bearing contact surfaces was unknown, full-scale prototype testing was necessary for better estimation of forces and the hysteresis characteristics.

5 FURTHER DEVELOPMENT

Because physical construction profoundly influences performance, ASCE 7-16 [15] Chapter 17 seismic isolation provisions require prototype testing. Future prototypes of this elliptical system may place sacrificial wind restraints at corners of the panels and U-shaped flexural plates spanning panel joints to assess practical details. Future prototypes may characterize additional contact bearing surfaces in dynamic tests and model long-term performance of wood. To address questions common to isolation systems, the performance-based provisions of ASCE 7-16 [15] provide the general framework to analytically and physically develop complete isolation systems.

ACKNOWLEDGEMENT

The U.S. Forest Service, in cooperation with the University of Wisconsin—Milwaukee, funded this research through the Wood Innovations Grant Number: 2016-DG-11420004-170.

REFERENCES

[1] Ceccotti A. and Follesa M., Seismic Behavior of Multi-Storey XLam Buildings, *International Workshop on Earthquake Engineering on Timber Structures*, pages 81-95, COST E29- European Cooperation in the Field of Scientific and Technical Research: Coimbra, Portugal, 2006.

[2] Ceccotti A., Sandhaas C., Okabe M., Yasumura M., Minowa C., and Kawai N., SOFIE project – 3D shaking table test on a seven-storey full-scale cross-laminated timber building. *Earthquake Engineering & Structural Dynamics*, 42(13): 2003-2021, 2013.

[3] Pei S., Berman J., Dolan J.D., van de Lindt J.W., Ricles J., Sause R., Blomgren H.-E., Popovski M., and Rammer D.R. Progress on the development of seismic resilient Tall CLT Buildings in the Pacific Northwest. In: *Proceedings of the 2014 World Conference on Timber Engineering*, Quebec City, Canada, 2014.

[4] Pei S., van de Lindt J.W., Popovski M., Berman J.W., Dolan J.D., Ricles J., Sause R., Blomgren H.-E., and Rammer D.R., Cross-Laminated Timber for Seismic Regions: Progress and Challenges for Research and Implementation. *Journal of Structural Engineering*, 142(4): E2514001, 2016.

[5] Amini M.O., van de Lindt J.W., Rammer D.R., Pei S., Line P., and Popovski M., Systematic experimental investigation to support the development of seismic performance factors for cross laminated timber shear wall systems. *Engineering Structures*, 172: 392-404, 2018.

[6] Federal Emergency Management Agency (FEMA): Quantification of Building Seismic Performance Factors, Federal Emergency Management Agency (FEMA), Washington D.C., 2009.

[7] Pei S., van de Lindt J.W., Ricles. J.M., Sause R., Berman J., Ryan K., Dolan J.D., Buchanan A.H., Robinson T., McDonnel E., Blomgren H.-E., Popovski M., and Rammer D.R., Development and Full-Scale Validation of Resilience-Based Seismic Design of Tall Wood Buildings: The NHERI Tallwood Project, *Journal Name: Proceedings of the New Zealand Society for Earthquake Engineering Annual Conference, April 27-29, Wellington, New Zealand*, 2017.

[8] Pei S., van de Lindt J.W., Barbosa A., Berman J., McDonnell E., Dolan J.D., Zimmerman R.B., Sause R., Ricles J., and Ryan K. Full-Scale Shake Table Test of Mass-Timber Building With Resilient Post-Tensioned Rocking Walls. In: *World Conference on Timber Engineering*, Seoul, Republic of Korea, 2018.

[9] Pei S., Berman J., Ryan K., Ricles J., Sause R., Dolan J.D., and van de Lindt J.W. Natural Hazards Engineering Research infrastructure (NHERI) Tall Wood Project. Available from: http://nheritallwood.mines.edu/index.html 2018 [cited 2020 September 8].

[10] Housner G.W., The behavior of inverted pendulum structures during earthquakes. *Bulletin of the seismological society of America*, 53(2): 403-417, 1963.

[11] Restrepo J. and Rahman A., Seismic Performance of Self-Centering Structural Walls Incorporating Energy Dissipators. *Journal of Structural Engineering*, 133(11): 1560-1570, 2007.

[12] Ganey R., Berman J., Akbas T., Loftus S., Daniel Dolan J., Sause R., Ricles J., Pei S., van de Lindt J.W., and Blomgren H.-E., Experimental Investigation of Self-Centering Cross-Laminated Timber Walls. *Journal of Structural Engineering*, 143(10): 04017135, 2017.

[13] Akbas T., Sause R., Ricles J.M., Ganey R., Berman J., Loftus S., Dolan J.D., Pei S., Lindt J.W.v.d., and Blomgren H.-E., Analytical and Experimental Lateral-Load Response of Self-Centering Posttensioned CLT Walls. *Journal of Structural Engineering*, 143(6): 04017019, 2017.

[14] Kovacs M. and Wiebe L. Controlled Rocking Cross-Laminated Timber Walls for Regions of Low-to-Moderate Seismicity. In: *World Conference on Timber Engineering (WCTE 2016)*, Vienna, Austria, 2016.

[15] American Society of Civil Engineers (ASCE) and Structural Engineering Institute (SEI), Minimum Design Loads and associated Criteria for Buildings and Other Structures (ASCE/SEI 7-16), American Society of Civil Engineers: Reston, VA, USA, 2017.

[16] Jangid R.S. and Londhe Y.B., Effectiveness of Elliptical Rolling Rods for Base Isolation. *Journal of Structural Engineering*, 124(4): 469-472, 1998.

[17] McVitty W. and Taylor A., Chapter 15: Seismically Isolated Structures, In R. Pekelnicky, editor, *2015 NEHRP Recommended Seismic Provisions: Design examples. FEMA P-1051*, pages (15)1-58. Federal Emergency Management Agency (FEMA), Washington D.C., 2016.

[18] Londhe Y.B. and Jangid R.S., Dynamic response of structures supported on elliptical rolling rods. *Doboku Gakkai Ronbunshu*, 612: 11-20, 1999.

[19] Lo Ricco M., Ghorbanpoor A., Pei S., Rammer D.R., Begel M., Bridwell J., and Zimmerman R.B., Prototyping a Passively Self-Centering Cross-Laminated Timber Rocking Wall System: Analytical and Experimental Investigation. *Wood Design Focus*, 28(2): 23-39, 2018.

[20] Structural Engineers Association of California (SEAOC). Seismic Design Map Tool. 2020 [cited 2020 August 12].

[21] Lo Ricco M.: Prototyping Elliptically Profiled Inverted Pendulum Walls in Cross-Laminated Timber (CLT) for Passive Sellf-Centering and Seismic Resiliency. Civil & Environmental Engineering, Doctor of Philosophy in Engineering. University of Wisconsin-Milwaukee, Milwaukee, Wisconsin, 2019.

In: Proceedings of the World Conference on Timber Engineering, August 9-12, 2021, Santiago, Chile.
Paper No: TE0321.